Optics Letters

Integrated photonic molecule Brillouin laser with a high-power sub-100-mHz fundamental linewidth

Kaikai Liu,[1] Jiawei Wang,[1] Nitesh Chauhan,[1] Mark W. Harrington,[1] Karl D. Nelson,[2] and Daniel J. Blumenthal[1,*]

[1]Department of Electrical and Computer Engineering, University of California Santa Barbara, Santa Barbara, California, USA
[2]Honeywell Aerospace, Plymouth, Minnesota, USA
*danb@ucsb.edu

Received 17 August 2023; revised 28 October 2023; accepted 5 November 2023; posted 10 November 2023; published 19 December 2023

Photonic integrated lasers with an ultra-low fundamental linewidth and a high output power are important for precision atomic and quantum applications, high-capacity communications, and fiber sensing, yet wafer-scale solutions have remained elusive. Here we report an integrated stimulated Brillouin laser (SBL), based on a photonic molecule coupled resonator design, that achieves a sub-100-mHz fundamental linewidth with greater than 10-mW output power in the C band, fabricated on a 200-mm silicon nitride (Si_3N_4) CMOS-foundry compatible wafer-scale platform. The photonic molecule design is used to suppress the second-order Stokes (S2) emission, allowing the primary lasing mode to increase with the pump power without phase noise feedback from higher Stokes orders. The nested waveguide resonators have a 184 million intrinsic and 92 million loaded Q, over an order of magnitude improvement over prior photonic molecules, enabling precision resonance splitting of 198 MHz at the S2 frequency. We demonstrate S2-suppressed single-mode SBL with a minimum fundamental linewidth of 71±18 mHz, corresponding to a 23±6-mHz^2/Hz white-frequency-noise floor, over an order of magnitude lower than prior integrated SBLs, with an ∼11-mW output power and 2.3-mW threshold power. The frequency noise reaches the resonator-intrinsic thermo-refractive noise from 2-kHz to 1-MHz offset. The laser phase noise reaches −155 dBc/Hz at 10-MHz offset. The performance of this chip-scale SBL shows promise not only to improve the reliability and reduce size and cost but also to enable new precision experiments that require the high-speed manipulation, control, and interrogation of atoms and qubits. Realization in the silicon nitride ultra-low loss platform is adaptable to a wide range of wavelengths from the visible to infrared and enables integration with other components for systems-on-chip solutions for a wide range of precision scientific and engineering applications including quantum sensing, gravitometers, atom interferometers, precision metrology, optical atomic clocks, and ultra-low noise microwave generation.

https://doi.org/10.1364/OL.503126

Introduction. Photonic integrated ultra-narrow linewidth, ultra-low phase noise lasers, with a high output power, have the potential for low cost, size, weight, and power solutions for a wide range of precision scientific and commercial applications, including coherent communications [1,2], fiber-optic sensing [3–5], atomic and quantum sensing [6], atomic clocks [7], and ultra-low-noise microwave generation [8–10]. The fundamental linewidth plays a key role in applications that have stringent requirements on the laser frequency noise from carrier from 10 kHz out to multiple MHz. For example, the laser manipulation and interrogation of atoms and qubits require ultra-low noise at high offset-from-carrier frequencies to minimize unwanted interactions with neighboring hyperfine atomic transitions, motional sidebands, and fast pulse sequencing used in ion and neutral atom manipulation. The intermodulation distortion of laser noise can set a fundamental limit in the stability of atomic frequency [11], and the phase noise in optical frequency division can set the performance limit for microwave signal generation [12,13]. Traditionally, these systems employ costly external cavity lasers and are relegated to table-top systems and utilize frequency doubling of near-infrared (NIR) lasers. Other desirable features include a high output power, a low threshold power, and fabrication in wafer-scale CMOS foundry compatible processes that can be used to integrate other components on chip and allow designs that operate from the visible to NIR such as the ultra-low loss silicon nitride platform [14–17].

In particular, the physical processes involved in the stimulated Brillouin laser (SBL) emission result in a large suppression of the pump fundamental linewidth [18–20]. To date, waveguide-based SBLs have been integrated in the silicon nitride CMOS foundry compatible platform at NIR and visible wavelengths [21,22], with fundamental linewidths as low as 720 mHz. The fundamental linewidth and the output power are limited due to the cascaded Brillouin emission where higher-order emission modes lead to clamping of photon population in the primary mode and phase noise feedback from higher-order modes [19]. Inhibition of the higher-order Stokes emission such as second-order Stokes (S2) [23] has been employed with silicon nitride waveguide SBLs through sidewall grating modulation of a silicon nitride ring resonator to split the S2 resonance [24]. In this previous work, the low resonator Q limited the resolution of S2 line splitting, and the fundamental linewidth was not characterized. Suppressed S2 in a non-integrated tapered-fiber coupled bulk optic silica microtoroid resonator achieved a fundamental linewidth of 245 mHz at a high output power of 126 mW [25].

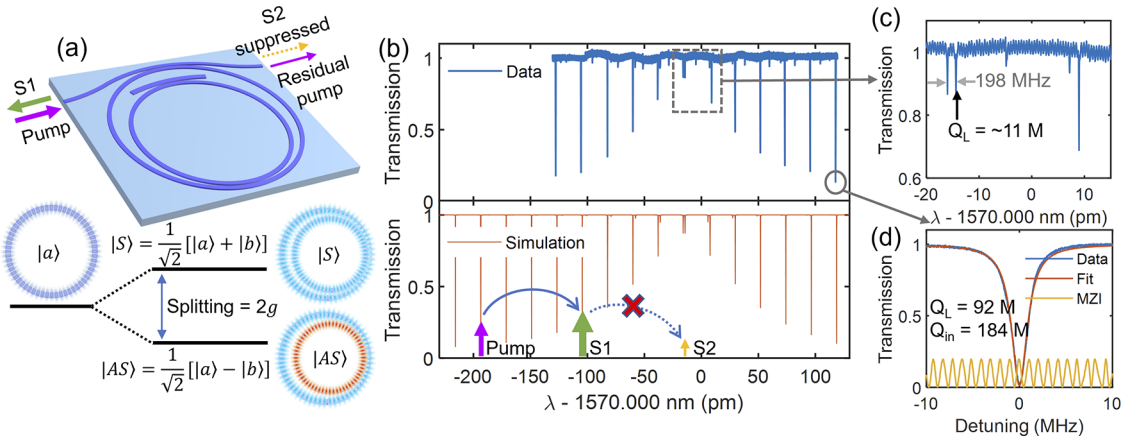

Fig. 1. S2-suppressed design. (a) Coupled-ring resonator with split resonances due to mode coupling for S2 suppression. Split modes correspond to symmetric $|S\rangle$ and asymmetric $|AS\rangle$ hybrid modes. (b) Normalized transmission shows one split resonance and other non-split resonances near 1570 nm. (c) Zoom-in of the split resonance. (d) Q and linewidth measurement of the non-split resonance.

However, the limited resonator Q of 31 million resulted in an ~49-mW threshold and unwanted output saturation where the laser most likely loses S2 suppression. To reach below the sub-100-mHz fundamental linewidth requires cascaded Brillouin inhibition approaches that leverage the performance of ultrahigh Q integrated waveguide resonators in a CMOS foundry compatible platform [15,16,26,27]. This paper focuses on integrated Brillouin lasers. Sub-100-mHz fundamental linewidth has been demonstrated using self-injection locking to silicon nitride coil resonators [28]. However, SIL has issues with long-term laser stability which is not an issue with the SBL.

In this paper, we report an S2-suppressed Brillouin laser based on a photonic-molecule integrated waveguide resonator design that achieves a fundamental linewidth of 71±18 mHz, corresponding to 23±6-mHz^2/Hz white-frequency noise floor in the C band with an ~11-mW output power and a 2.3-mW optical threshold power. Additionally, the laser phase noise is measured at −155 dBc/Hz at 10-MHz offset. These results represent over an order of magnitude improvement in fundamental linewidth and phase noise over previous waveguide integrated Brillouin lasers, to the best of our knowledge. The nested resonator is fabricated in a 200-mm silicon nitride (Si_3N_4) CMOS-foundry compatible wafer-scale platform and has a 184 million intrinsic and 92 million loaded Q, enabling a resonance splitting of 198 MHz at the S2 offset frequency and ultra-low phase noise operation. Increasing the pump power from above the threshold to 170 mW (~70 times the 2.3-mW threshold), no higher-order Stokes are observed, confirming a single-mode operation. The frequency noise measurements are characterized to have a noise floor that is low enough to measure the white frequency noise floor from 1- to 10-MHz offset. Comparing the measured frequency noise spectra to the modeled thermo-refractive noise (TRN), the measurements match the TRN from 10 kHz to 1. This nested ring photonic-molecule approach is advantageous compared to other approaches with a resulting resonator Q above 100 million, a well-defined resonance splitting controlled by the ring–ring coupling gap that is fabrication-tolerant to a few microns and enables a Vernier effect that repeats every ~0.35 nm.

Photonic-molecule Brillouin laser design. The photonic molecule resonator is based on a nested double-ring structure (Fig. 1(a)) that couples the modes of the two ring resonators to produce the resonance splitting at the desired Brillouin S2 frequency shift. The transverse magnetic Si_3N_4 waveguide is 11-μm wide by 80-nm thick based on the design and loss mitigation techniques as reported in [15]. The outer ring, where Brillouin lasing occurs, has a radius of 11.787 mm, designed to satisfy the Brillouin phase matching condition with four times the free spectral range (FSR) equal to the Brillouin shift [15,22]. The inner ring radius is 10.50 mm. The coupling structures are single point coupling without pulley-coupler type design features such as a change in the ring curvature or the bus waveguide bending (see Fig. S2(a) in Supplement 1 Section 3). A main advantage of our ultra-low loss platform with dilute optical mode is that it enables this simple single-point-coupling resonator design without complicated design features. The gaps of the coupling structures are chosen with the guidance of the coupling simulation of the large-size ring resonator (Supplement 1 Section 4). The bus-ring gap of the outer ring is 5.2 μm for critical coupling, and the ring-ring gap is 5.0 μm to introduce coupling between the rings that creates a resonance splitting of ~100 MHz. To further increase the suppression of the S2 emission, we add an auxiliary bus waveguide with a bus-ring gap of 2.5 μm to the inner ring for over coupling to intentionally add loss to the inner ring resonances, resulting in a decreased loaded Qs at the split resonance, which further increases the suppression of S2 lasing.

Figure 1(b) shows a spectral scan with different FSRs of the two modes creating a split resonance at 1569.986 nm. As shown in Fig. 1(b), to achieve S2 suppression, the pump laser is aligned with the non-split resonance that is 8 FSRs away from the split resonance. Figure 1(b) also shows the simulated transmission (orange line in Fig. 1(b)) of the coupled resonator using a matrix-based coupled mode theory [29,30] with the measured Q values and the splitting rate $g = 198/2 = 99$ MHz and agrees well with the measured spectral scanning trace (blue line in Fig. 1(b)). The split and non-split resonances are measured using a radio frequency calibrated fiber Mach–Zehnder interferometer (MZI) [27]. The non-split resonance Q is measured to be 184 million intrinsic and 92 million loaded around 1570 nm (Fig. 1(d)), while the resonance split at 1569.986 nm (Fig. 1(c)) is measured to be 198 MHz with a loaded Q of ~11 million.

Linewidth and frequency noise measurement. For the S2-suppressed non-cascaded-emission Brillouin laser, the first-order Stokes (S1) fundamental linewidth follows the modified

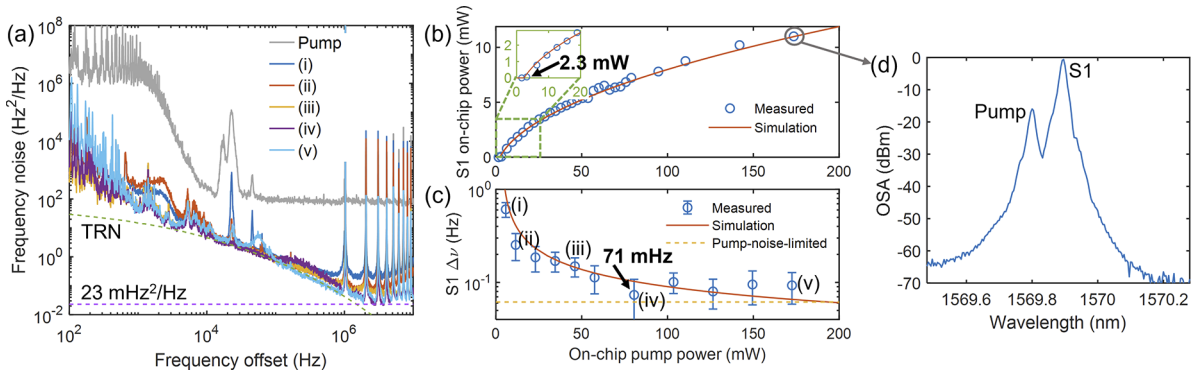

Fig. 2. S2-suppressed SBL threshold, output power, and fundamental linewidth measurement. (a) OFD frequency noise at different pump powers. (b) S1 on-chip power versus pump power with measured 2.3-mW threshold. (c) Fundamental linewidth versus pump power. The pump noise limited linewidth is indicated by yellow dash. (d) S2-suppressed SBL on an OSA at 170-mW pump power. S1, first-order Stokes; S2, second-order Stokes; OFD, optical frequency discriminator; OSA, optical spectrum analyzer.

Schawlow–Townes linewidth with an enhancement factor (α) induced by Brillouin gain amplitude-phase coupling [19,20],

$$\Delta\nu_{S1,ST} = \frac{n_{th}\hbar\omega^3}{4\pi Q_L Q_{ex} P_{S1}}(1+\alpha^2), \tag{1}$$

where $n_{th} = 1/\left[\exp\left(\frac{\hbar\Omega}{kT}\right) - 1\right]$ is the photon thermal quanta ($\cong$573 at 300 K), Ω is the acoustic wave frequency, ω is the Brillouin laser frequency, Q_L and Q_{ex} are the resonator loaded Q and coupling external Q, P_{S1} is the S1 output power, and α is the linewidth enhancement factor due to the deviation from perfect phase matching. For cascaded emission SBLs, S1 emission clamps at the onset (threshold) of S2. The S1 fundamental linewidth reaches a minimum due to saturation of the photon number without higher-order Stokes phase noise feedback [19, 31],

$$\Delta\nu_{\min} = \frac{n_{th}\mu}{2\pi}, \tag{2}$$

where $\mu = h\nu v_g^2 G_B/2L$ is the cavity Brillouin gain rate, v_g is the group velocity, G_B is the material Brillouin gain, and L is the cavity length (see [19] and Supplement 1 Section 2 for detailed derivation of Eqs. (1) and (2)).

To demonstrate S2 suppression, a Velocity TLB-6700 tunable laser is locked to the non-split resonance located 8 FSRs away from the split resonance, using the Pound–Drever–Hall technique [32], where the pump laser is amplified by an erbium-doped fiber amplifier (EDFA) before a fiber circulator and fiber-to-chip edge coupling with ~4-dB loss at the edge coupling (see experimental setup in Supplement 1 Fig. S2(a)). The S1 output power is coupled to a fiber circulator at the reflection port and measured on an optical spectrum analyzer (OSA). The S1 threshold is measured to be 2.3 mW, and the pump power is increased up to 170 mW without observation of S2 (Fig. 2(d)), confirming single-mode operation. Due to the ~4-dB edge loss and the maximum 27-dBm EDFA output power, the 170-mW on-chip pump power is the maximum that was reached.

The frequency noise and the fundamental linewidth are measured using a fiber MZI optical frequency discriminator (OFD) [22], and the fundamental linewidth $\Delta\nu_F$ is calculated from the white-frequency-noise floor, $\Delta\nu_F = \pi S_w$. The S1 frequency noise and the output power are measured as a function of the increased pump power (Figs. 2(a) and 2(c)) demonstrating linewidth narrowing and the expected square-root law increase in the S1 power [19]. At 80-mW on-chip pump power (data trace (iv) in Fig. 2(1)), the white-frequency-noise floor is reduced to 23±6 mHz²/Hz, corresponding to 71±18 mHz, and at pump power above 80 mW the S1 fundamental linewidth is measured to be on average 82±7 mHz (Fig. 2(c)). To better visualize the white frequency noise at high-frequency offsets (1–10 MHz), the frequency noise spectra are plotted with the offset in the linear scale, shown in Fig. S2(b) in Supplement 1 Section 3. The measured S1 output power and linewidth are plotted together with the simulated curves in Figs. 2(b) and 2(c), where the S2-suppressed modeling follows [19] and is described in detail in Supplement 1 Section 2.

We calculate the equivalent single-sideband phase noise for the data trace (v) in Fig. 2(a) at an on-chip pump power of 170 mW (Fig. 3). At frequencies from 10 kHz to 1 MHz, the laser frequency phase noise follows the resonator-intrinsic TRN [33,34]. The equivalent phase noise reaches −155 dBc/Hz at 10-MHz offset before hitting the OFD noise floor. The OFD measurement noise floor is carefully characterized by sampling the noise signal without any optical input and converting it into an equivalent frequency and phase noise spectrum, shown as the pink trace in Fig. 3. Above the 10-MHz offset, the measured phase noise is limited by the OFD noise floor (Supplement 1 Section 3 for OFD noise floor details).

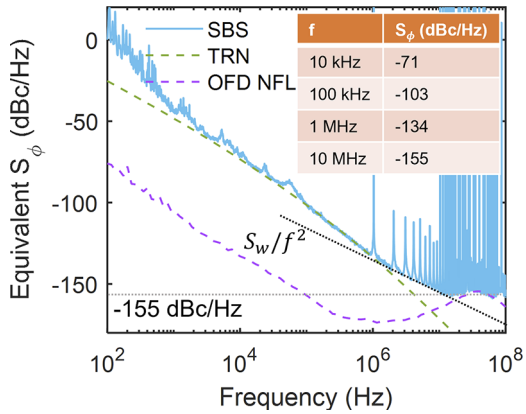

Fig. 3. Single sideband phase noise is calculated from the frequency noise trace (v) at the pump power of 170 mW in Fig. 2(a), where the phase noise reaches −155 dBc/Hz at 10 MHz. Above 10 MHz, the measured phase noise is limited by OFD noise floor (NFL). S_w, white frequency noise.

Conclusion and discussion. We report an ultra-low phase noise, high output power SBL that uses a photonic-molecule integrated resonator design to suppress the higher order Stokes modes. We achieve a fundamental linewidth of 71±18 mHz (corresponding to 23±6-mHz^2/Hz white-frequency noise floor) and −155-dBc/Hz phase noise at 10 MHz, with ∼11-mW output power at the on-chip pump power of 170 mW. The photonic molecule waveguide resonators are fabricated in a 200-mm wafer-scale CMOS-foundry platform and have a measured 184 million intrinsic and 92 million loaded Qs at the non-split resonances and a resonance splitting of 198 MHz at the S2 wavelength. There are several advantages with our nested resonator photonic-molecule SBL design for higher-order Stokes suppression. First, the S2 resonance splitting can be determined by the ring–ring coupling gap, which is on the order of a few microns and is within the fabrication error tolerance of our lithography and chemical etching. Second, the auxiliary bus coupling to the inner ring further contributes to the S2 suppression by decreasing the Qs of the split resonances. Third, the coupled rings produce a Vernier effect for the resonance splitting such that the split periodically appears every ∼0.35 nm. This repeating behavior of split resonances has been well studied [35]. This design has fabrication tolerance advantages over the nano-modulation features used in prior resonator grating structures [24].

Important to the validation of the laser noise is the fact that the SBL frequency noise reaches the intrinsic TRN of the photonic molecule resonators (green dash in Fig. 2(a)). Additionally, this TRN limit is above the noise floor of our frequency noise measurement system (solid purple Fig. 3). Another consideration is the pump laser noise which sets a limit on how narrow the SBL fundamental linewidth can reach. The transferred pump frequency noise limited linewidth is calculated to be 62 mHz (yellow dash in Fig. 2(c)), using the formula in Ref. [18] (see Supplement 1 Section 2). Before reaching the pump-transferred-noise-limited linewidth, the linewidth continues to reduce with increasing output laser power (Eq. (1)). However, with S2 suppression, S1 does not increase linearly with input pump power (P_{in}). The resulting increase proportional to $\sqrt{P_{in}}$ leads to a decreasing conversion efficiency at high pump power [19],

$$P_{S1} = \frac{4\gamma_{ex}^2}{\gamma^2}\left(\sqrt{P_{th}P_{in}} - P_{th}\right) \cong \frac{4\gamma_{ex}^2}{\gamma^2}\sqrt{P_{th}P_{in}}, \tag{3}$$

where γ_{ex} and γ are the resonator coupling loss rate and total loss rate and P_{th} is the threshold. This results in a conversion efficiency $\eta_{S1} \cong \frac{4\gamma_{ex}^2}{\gamma^2}\sqrt{P_{th}/P_{in}}$ that decreases with the pump power P_{in}, which leads to the low conversion efficiency of 6.5% at the 170-mW pump power and also affects the fundamental linewidth narrowing (Fig. 2(b)). To avoid this $\sqrt{P_{in}}$ dependence we can leverage the fact that the S2 emission output power with S3 suppression increases linearly with pump power (see Supplement 1 Section 2 on S3 suppression). We investigated S3 suppression with S2 as the SBL output for improved power conversion efficiency and linewidth reduction. However,the four-wave mixing parametric process inhibits the increase of S2 output power at the 55-mW pump power (Supplement 1 Section 6). Future work will include investigation and suppression of the unwanted four-wave mixing process. In conclusion, the exceptional ultra-narrow fundamental linewidth and high output power of the photonic molecule suppressed the S2 chip-scale SBL, showing promise not only to improve the reliability and reduce size and cost but also enable precision atomic and quantum high-speed manipulation, control, and interrogation, impacting future atomic and quantum sensing, computing and precision microwave applications.

Funding. Army Research Office (W911NF-23-1-0179); Microsystems Technology Office (HR0011-22-2-0008); Advanced Research Projects Agency - Energy (DE-AR0001042).

Disclosures. The authors declare no conflicts of interest.

Data availability. Data underlying the results presented in this paper are not publicly available at this time but may be obtained from the authors upon reasonable request.

Supplemental document. See Supplement 1 for supporting content.

REFERENCES

1. K. Kikuchi, J. Lightwave Technol. **34**, 157 (2016).
2. D. J. Blumenthal, H. Ballani, R. O. Behunin, *et al.*, J. Lightwave Technol. **38**, 3376 (2020).
3. P. Lu, N. Lalam, M. Badar, *et al.*, Appl. Phys. Rev. **6**, 041302 (2019).
4. E. Ip, J. Fang, Y. Li, *et al.*, J. Opt. Commun. Netw. **14**, A61 (2022).
5. A. Mecozzi, C. Antonelli, M. Mazur, *et al.*, J. Lightwave Technol. **41**, 3350 (2023).
6. C. Xu, L. Zhang, S. Huang, *et al.*, Photonics Res. **7**, A14 (2019).
7. A. D. Ludlow, M. M. Boyd, J. Ye, *et al.*, Rev. Mod. Phys. **87**, 637 (2015).
8. J. Li, H. Lee, and K. J. Vahala, Nat. Commun. **4**, 2097 (2013).
9. P. A. Morton and M. J. Morton, J. Lightwave Technol. **36**, 5048 (2018).
10. B. Wang, Z. Yang, X. Zhang, *et al.*, Nat. Commun. **11**, 3975 (2020).
11. G. Santarelli, C. Audoin, A. Makdissi, *et al.*, IEEE Trans. Ultrason., Ferroelect., Freq. Contr. **45**, 887 (1998).
12. J. Liu, E. Lucas, A. S. Raja, *et al.*, Nat. Photonics **14**, 486 (2020).
13. T. M. Fortier, M. S. Kirchner, F. Quinlan, *et al.*, Nat. Photonics **5**, 425 (2011).
14. D. J. Blumenthal, R. Heideman, D. Geuzebroek, *et al.*, Proc. IEEE **106**, 2209 (2018).
15. K. Liu, N. Jin, H. Cheng, *et al.*, Opt. Lett. **47**, 1855 (2022).
16. M. W. Puckett, K. Liu, N. Chauhan, *et al.*, Nat. Commun. **12**, 934 (2021).
17. N. Chauhan, J. Wang, D. Bose, *et al.*, Opt. Express **30**, 6960 (2022).
18. A. Debut, S. Randoux, and J. Zemmouri, Phys. Rev. A **62**, 023803 (2000).
19. R. O. Behunin, N. T. Otterstrom, P. T. Rakich, *et al.*, Phys. Rev. A **98**, 023832 (2018).
20. Z. Yuan, H. Wang, L. Wu, *et al.*, Optica **7**, 1150 (2020).
21. N. Chauhan, A. Isichenko, K. Liu, *et al.*, Nat. Commun. **12**, 4685 (2021).
22. S. Gundavarapu, G. M. Brodnik, M. Puckett, *et al.*, Nat. Photonics **13**, 60 (2019).
23. M. Merklein, I. V. Kabakova, T. F. S. Büttner, *et al.*, Nat. Commun. **6**, 6396 (2015).
24. M. Puckett, D. Bose, K. Nelson, *et al.*, in *CLEO: Science and Innovations* (Optical Society of America, 2019), pp. SM4O-1.
25. Y. Qin, S. Ding, M. Zhang, *et al.*, Opt. Lett. **47**, 1638 (2022).
26. W. Jin, Q.-F. Yang, L. Chang, *et al.*, Nat. Photonics **15**, 346 (2021).
27. H. Lee, T. Chen, J. Li, *et al.*, Nat. Photonics **6**, 369 (2012).
28. B. Li, W. Jin, L. Wu, *et al.*, Opt. Lett. **46**, 5201 (2021).
29. M. C. M. M. Souza, G. F. M. Rezende, L. A. M. Barea, *et al.*, Opt. Express **24**, 18960 (2016).
30. J. Wang, K. Liu, A. Isichenko, *et al.*, Opt. Lett. **48**, 2373 (2023).
31. J. Li, H. Lee, T. Chen, *et al.*, Opt. Express **20**, 20170 (2012).
32. E. D. Black, Am. J. Phys. **69**, 79 (2001).
33. J. H. Dallyn, K. Liu, M. W. Harrington, *et al.*, Phys. Rev. A **105**, 043506 (2022).
34. K. Liu, N. Chauhan, J. Wang, *et al.*, Optica **9**, 770 (2022).
35. O. Schwelb, Opt. Commun. **281**, 1065 (2008).